Journal of Applied Polymer Science

# Influence of $TiO_2$ nanoparticles on nonisothermal crystallization of PP in a wide range of cooling rates analyzed by fast scanning DSC

**Buncha Suksut,[1] Alois K. Schlarb[1,2,3]**

[1]Chair of Composite Engineering, University of Kaiserslautern, Kaiserslautern 67663, Germany
[2]Research Center OPTIMAS, University of Kaiserslautern, Kaiserslautern 67663, Germany
[3]INM – Leibniz Institute for New Materials, Saarbrucken, 66123, Germany
Correspondence to: B. Suksut (E-mail: buncha.suksut@mv.uni-kl.de)

**ABSTRACT:** The influence of titanium dioxide ($TiO_2$) nanoparticles on the crystallization behavior of polypropylene was investigated by conventional differential scanning calorimetry (DSC) and fast scanning DSC measurements. The data obtained from both methods were estimated for the first time using the Lauritzen-Hoffmann equation to analyze the behavior over a wide cooling range under nonisothermal conditions. This provides more reliable values of nucleation parameters ($K_g$) and surface free energy ($\sigma_e$). The variation of the effective energy ($\Delta E$) was determined with the Kissinger method. Regardless of the cooling rate, both $K_g$ and $\sigma_e$ indicate the role of titania as a nucleating agent enhances the crystallization rate. However, the $\Delta E$ denotes that $TiO_2$ acts as an obstacle to the mobility of chain segments at cooling rates below 150 °C/s, while, in contrast, the presence of titania enhances the chain mobility at cooling rates above 150 °C/s. © 2016 Wiley Periodicals, Inc. J. Appl. Polym. Sci. **2016**, *133*, 43944.

**KEYWORDS:** composites; crystallization; differential scanning calorimetry (DSC); nanoparticles; nanowires and nanocrystals; polyolefins

Received 12 February 2016; accepted 13 May 2016
**DOI: 10.1002/app.43944**

## INTRODUCTION

Polypropylene, PP, is one of the most widely used and fastest growing classes of thermoplastic polymers in numerous industries. It exhibits a good balance between physical and mechanical properties as well as easy processability at a relatively low cost. However, the use of PP is still limited by its comparatively low modulus and stiffness in comparison with engineering plastics.[1] To overcome these limitations, one of the most useful methods is the incorporation of reinforcing fillers such as glass, carbon, and aramid fibers as well as natural fibers[2,3] or synthetic fibers[4] to enhance the properties of polymeric materials.[5] In recent years, research also investigated the use of inorganic nanoparticles such as calcium carbonate ($CaCO_3$),[6] titania ($TiO_2$),[7] and silica ($SiO_2$)[8,9] to improve mechanical and functional properties of plastics.

In general, it is known that the mechanical properties of semicrystalline polymers are highly dependent on their morphological structure, which is governed by the respective crystallization processes undergone during production. Using thermoanalytical (TA) data, analysis of quiescent crystallization kinetics is usually performed under either isothermal or nonisothermal conditions. To elucidate the mechanism of crystallization in polymers, isothermal studies are state of the art. Crystallization kinetics of polymers have been commonly studied based on the Avrami equation[10–12] and the Lauritzen-Hoffmann theory.[13,14] While the Avrami equation and its modifications are used to describe the bulk crystallization kinetics of polymers, the Lauritzen-Hoffmann theory suggests that crystallization is controlled by nucleation and transport of macromolecules in the melt.[15]

Most investigations on crystallization are obtained from conventional DSC where the fastest applied cooling rate can not exceed 1 °C/s.[16] Experimental data about crystallization are only available in a narrow range of cooling and temperatures. This often leads to crystallization at low supercooling levels of the melt. Investigation of crystallization in cooling conditions relevant in polymer processing, which is beyond the capability of standard DSC, is not possible. Consequently, to reach higher cooling rates, high performance DSCs are required. Very few are described in the literature. Notable developments include the ultra-fast scanning calorimeters[17,18] and flash DSC 1.[19] The development of such high performance DSCs has helped to achieve breakthrough knowledge in the field of polymer crystallization in a much wider temperature/supercooling range than on application of DSC. This technique has given new insights into crystallization, melting behavior, glass transition, and

**Table I.** Sample Designation and Composition of PP-Based Nanocomposites

| | Composition, vol % | |
|---|---|---|
| Designation | PP | $TiO_2$ |
| PP-V0 | 100 | — |
| PP-T-V1 | 99 | 1 |
| PP-T-V4 | 96 | 4 |

structural reorganization under fast cooling of various polymers such as PA 6,[20] PA 11,[21,22] PBT,[23,24] PET,[24] PLA,[25,26] PTFE,[27] PB,[27,28] and iPP.[23–26,29–32]

While the conventional DSC is accepted for characterization of certain material properties, the flash DSC allows us to better understand the influence of nanofillers on the crystallization and the structure development under real processing conditions. The aim of this work was to investigate the crystallization of isotactic PP (iPP) containing $TiO_2$ nanoparticles by using conventional differential scanning calorimetry (DSC), and flash DSC. To the best of our knowledge, we applied the Lauritzen-Hoffmann theory for the first time to our materials and analyzed the effects of $TiO_2$ nanoparticles on the nonisothermal crystallization kinetics in a wider cooling range. The Kissinger model was used to verify the variation of the activation energy in a broader cooling range.

## EXPERIMENTAL

### Materials and Processes

PP (PP HD120 MO, Borealis GmbH, Burghausen, Germany) was used as a matrix material and titanium dioxide ($TiO_2$) nanoparticles (Hombitec RM130 F, Huntsman, Duisburg, Germany) as inorganic nanofillers.

PP nanocomposites were first prepared using an optimized co-rotating twin-screw extruder (Theysohn, Theysohn Extrusionstechnik GmbH, Salzgitter, Germany) followed by injection molding (Arburg Allround 420C, ARBURG GmbH + Co KG, Loßburg, Germany). The procedure is described in the literature[8] in detail. Using this procedure, three different materials were prepared as shown in Table I.

### Preparation of the Specimens

In order to study the crystallization, the center part of an injection-molded plate was cut into rectangular cuboids (Figure 1). Then, thin sections with a thickness of 30 μm were prepared from the center area of the rectangular samples using a rotation microtome (Hyrax M 25, Carl Zeiss MicroImaging GmbH, Jena, Germany) equipped with a steel blade.

### Differential Scanning Calorimetry

The measurements were performed on a DSC (TA Q20, TA instruments, Eschborn, Germany) equipped with the Refrigerated Cooling Systems 90 (RCS90). Indium was used as a reference material to calibrate both the temperature scale and the melting enthalpy before the samples were measured in alternate runs. To minimize thermal degradation each sample was used only once. Nitrogen gas was used for purging throughout the measurements. The weight of each specimen ranged from 5 to 10 mg. Each sample was placed in an aluminium pan and the pan was then completely sealed with an aluminium lid. For nonisothermal crystallization, the samples were heated to 220 °C at a rate of 0.17 °C/s and held for 180 s at this temperature. Then, the specimens were cooled to 0 °C at various cooling rates (from 0.03 to 0.67 °C/s).

### Flash DSC

Nonisothermal crystallization experiments were performed using a power compensation differential fast scanning chip calorimetry (FLASH DSC 1, Mettler Toledo, Gießen, Germany) in combination with a Huber Intracooler TC100. Dry nitrogen was used as a purge gas at a rate of 30 mL/min. The specimen was placed directly on the sensor. In order to provide a good thermal contact between the specimen and the sensor, the specimen was molten at a heating rate of 0.1 °C/s before the actual experiments. During the experiment, the samples were heated to 220 °C at a rate of 1000 °C/s, and were kept at this temperature for 0.1 s. Then, the specimen was cooled to −90 °C at various cooing rates. The heating and cooling rates as well as the holding time were chosen based on results published in Refs. 19,22.

## RESULT AND DISCUSSION

### Dependence of Cooling Rate on Crystallization Temperature

Figures 2 and 3 show the cooling curves of neat PP and PP/$TiO_2$−4 vol % obtained from conventional and flash DSCs, respectively. The plots show that only one crystallization process can occur at slower cooling rates. In addition, two different crystallization processes can be observed at cooling rates above 100 °C/s. The first crystallization process, at high temperature, can be interpreted as the crystallization of the α-phase of PP. The second one, at low temperature, is the formation of a mesophase.[23,33] No mesophase can be observed in the case of $TiO_2$-filled PP.

From the cooling curves in Figures 2 and 3, the peak of crystallization temperature ($T_p$) can be determined as shown in Figure 4. As expected, an increase in the cooling rate results in the

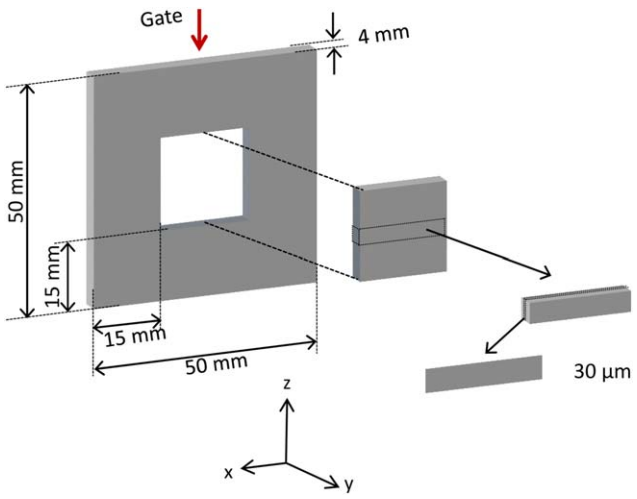


**Figure 1.** Preparation of specimens. [Color figure can be viewed in the online issue, which is available at wileyonlinelibrary.com.]

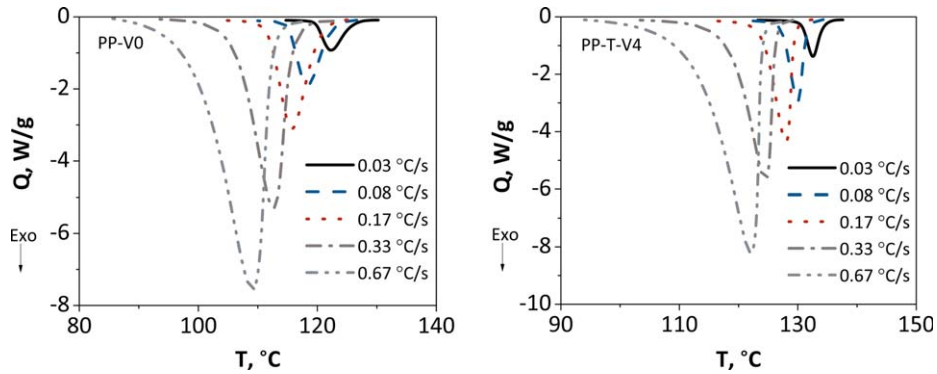


**Figure 2.** Cooling curves of (left) neat PP and (right) $TiO_2$-filled PP measured with DSC. [Color figure can be viewed in the online issue, which is available at wileyonlinelibrary.com.]

lowering of $T_p$ in all materials. The results show acceleration of crystallization with incorporation of $TiO_2$ nanoparticles, irrespective of the cooling rate. Furthermore, the mesophase of PP is obstructed by the presence of $TiO_2$ nanoparticles. Beyond the cooling rate of 700 °C/s, the observable crystallization and mesophase formation cannot be expressed in neat PP. However, crystallization still occurs at a cooling rate of up to approximately 2000 °C/s in $TiO_2$-filled PP.

With neat PP, the formation of a mesophase is faster than that of the crystallization of α-form. Therefore, the formation of the mesophase can occur during cooling in neat PP.[23] On the other hand, no formation of the mesophase in PP filled with $TiO_2$ nanoparticles indicates the much faster crystallization of α-form during cooling compared to the rate of mesophase formation.

### Crystallization Activation Energy by Kissinger Method

The activation energy ($\Delta E$), which is the energy required for the transportation of molecules from a molten state to a growing crystal surface for the nonisothermal crystallization of materials, can be determined using the Kissinger method[34] as follows:

$$\frac{d\left[\ln\left(\frac{\varnothing}{T_p^2}\right)\right]}{d\left(\frac{1}{T_p}\right)} = -\frac{\Delta E}{R} \tag{1}$$

where $T_p$, $R$, and $\varnothing$ are the peak of crystallization temperature, the universal gas constant and cooling rate, respectively. The plot of ln $(\varnothing/T_p^2)$ versus $1/T_p$ should be a straight line with a slope of $-\Delta E/R$.

The cooling rate range obtained from conventional DSC is very narrow. Therefore, the Kissinger plots tend to be straight, indicating single activation energy. In Figure 5, the data obtained from flash DSC at a higher cooling rate are an extension of conventional DSC. However, the Kissinger plots show a curvature which indicates that the effective activation energy decreases at a higher cooling rate (lower crystallization temperature).

As shown in Figure 5, three different regions can be defined in order to calculate the activation energy. The results thus obtained are summarized in Table II. Since the Kissinger method was formulated for heating experiments (i.e., positive heating rate values), the value of $\Delta E$ is always negative for the cooling process. As can be seen, the absolute values of $\Delta E$ for $TiO_2$-filled PP are greater than that for neat PP at lower cooling rates (below 150 °C/s, Period A and B). However, the absolute value of $\Delta E$ decreases by a factor of 2 in the presence of the $TiO_2$ nanoparticles at cooling rates above 150 °C/s (Period C). The result indicates that at lower cooling rates the PP molecular segments required more energy to rearrange in the presence of $TiO_2$, since the $TiO_2$ might hinder the mobility of chain segments. This may affect the spherulite growth rate of PP during crystallization. In contrast, it helps to increase the transportation ability of PP molecular chains during the crystallization process at higher cooling rates. This can be explained by the reduction of the activation energy, $\Delta E$ of $TiO_2$-filled PP at cooling rate above 150 °C/s as listed in Table II

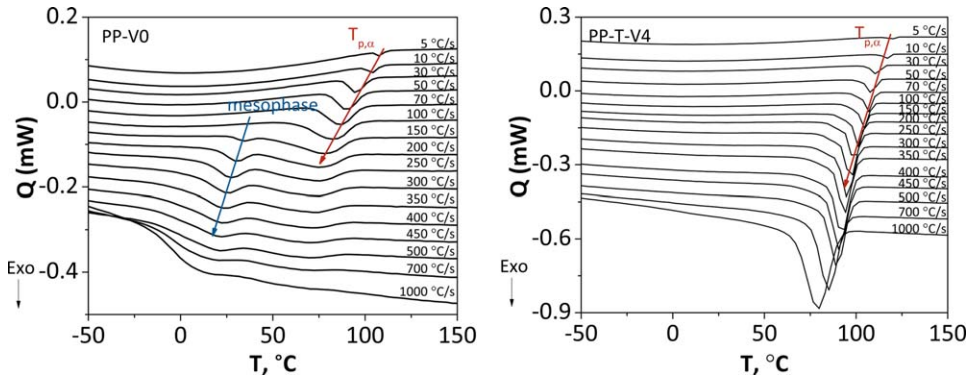


**Figure 3.** Cooling curves of (left) neat PP and (right) $TiO_2$-filled PP measured with FDSC. [Color figure can be viewed in the online issue, which is available at wileyonlinelibrary.com.]

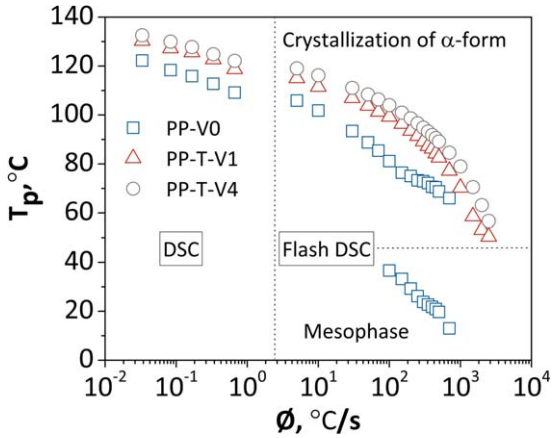


**Figure 4.** Peak of crystallization temperature as a function of the cooling rate. [Color figure can be viewed in the online issue, which is available at wileyonlinelibrary.com.]

### Continuous Cooling Transformation

Continuous cooling transformation (CCT) diagrams are widely used in metallurgy and solid-state phase transformations. These approaches have been applied to predict the polymer crystallization under any cooling condition.[35,36] Here, in order to construct the CCT diagram, the crystallization peak time and temperature, $t_p$ and $T_p$ were used, respectively. The CCT diagrams of materials are shown in Figure 6, where the crystallization point as a function of time and temperature is obtained at a constant cooling rate. If the presence of nanofiller is expected to increase the rate of the solidification/crystallization process, then the corresponding CCT curve will shift to a higher temperature. In the diagram, it can be observed that the crystallization point is reached at higher temperatures for the samples filled with $TiO_2$. This indicates that the $TiO_2$ nanoparticles accelerate the crystallization process of PP showing the nucleating effect during the crystallization process. This is a very useful tool for semi-crystalline polymer processing to predict the crystallization under any cooling conditions, i.e. under real industrial processing conditions.[37]

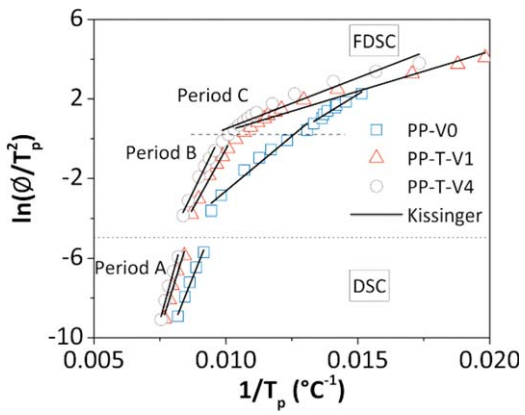


**Figure 5.** Kissinger plots for the evaluation of crystallization activation energy. [Color figure can be viewed in the online issue, which is available at wileyonlinelibrary.com.]

**Table II.** Activation Energy ($\Delta E$) from the Kissinger method

| Sample | Period | ∅ Range, °C/s | $\Delta E$, kJ/mol |
|---|---|---|---|
| PP-V0 | A | 0.03–0.67 | 398 |
| | B | 5–100 | 133 |
| | C | 150–700 | 98 |
| PP-T-V1 | A | 0.03–0.67 | 512 |
| | B | 5–100 | 288 |
| | C | 150–2500 | 48 |
| PP-T-V4 | A | 0.03–0.67 | 578 |
| | B | 5–100 | 328 |
| | C | 150–2500 | 62 |

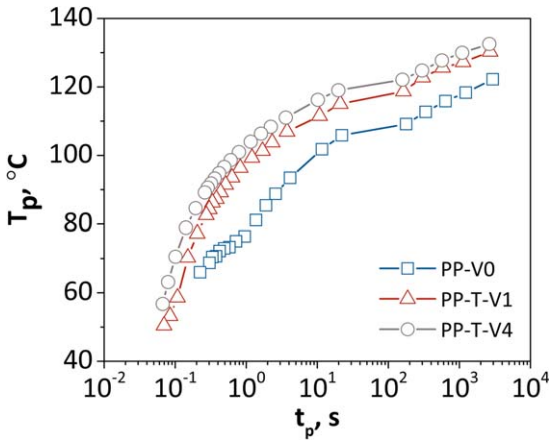


**Figure 6.** CCT diagram for neat and $TiO_2$-filled PP. [Color figure can be viewed in the online issue, which is available at wileyonlinelibrary.com.]

### Fold Surface Free Energy Based on the Lauritzen-Hoffmann Theory

Based on the Lauritzen-Hoffmann equation,[13,14] Chan and Isayev[38] replaced the growth rate ($G$) and a pre-exponential factor ($G_0$) with ($1/t_{1/2}$) and $(1/t_{1/2})_0$, respectively, in order to

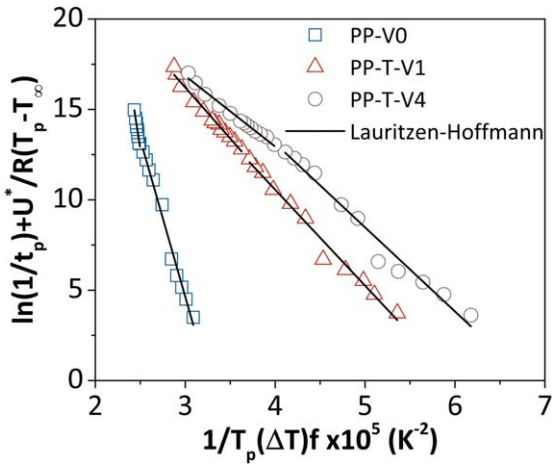


**Figure 7.** Lauritzen-Hoffmann plot for nonisothermal crystallization. [Color figure can be viewed in the online issue, which is available at wileyonlinelibrary.com.]

**Table III.** Parameters of Lauritzen-Hoffmann from Nonisothermal Crystallization

| Sample | [a]$T_m^0$, °C | Ø Range, °C/s | $T$ Range, °C | $K_g$ x $10^{-5}$, $K^2$ | $\sigma_e$, mJ/m$^2$ |
|---|---|---|---|---|---|
| PP-V0 | 213.6 | 0.03–100 | 81–122 | 17.4 | 33.1 |
| | | 150–700 | 66–76 | 32.1 | 61.1 |
| PP-T-V1 | 179.4 | 0.03–100 | 99–130 | 5.3 | 10.9 |
| | | 150–2500 | 55–96 | 5.4 | 10.9 |
| PP-T-V4 | 174.6 | 0.03–100 | 104–133 | 4.7 | 9.6 |
| | | 150–2500 | 57–101 | 3.9 | 8.1 |

[a] $T_m^0$ obtained from the authors' previous work.

describe the temperature dependence of the overall crystallization rate thus:

$$\left(\frac{1}{t_{1/2}}\right) = \left(\frac{1}{t_{1/2}}\right)0 \exp\left[\frac{-U^*}{R(T_i - T_\infty)}\right] \exp\left[\frac{-K_g}{T_i(\Delta T)f}\right] \quad (2)$$

where $(1/t_{1/2})_0$ is the pre-exponential factor, $U^*$ is the transport activation energy (6280 J/mol for PP), $R$ is the gas constant (8.314 J/(mol K), and $T_i$ is crystallization temperature. $f$ is the correction factor related to temperature, usually described as $f = 2T_i/(T_m^0 + T_i)$ to account for the variation in the heat of fusion per unit volume of crystal, $\Delta h_f$ ($1.93 \times 10^8$ J/m$^3$). $T_\infty$ is the theoretical temperature at which all motion associated with viscous flow ceases, defined as $T_\infty = T_g - 30$ K. $K_g$ is the nucleation constant and can be expressed as

$$K_g = \frac{4b_0\sigma\sigma_e T_m^0}{k_B(\Delta h_f)} \quad (3)$$

where $b_0$ is the layer thickness (6.26 x $10^{-10}$ m), $\sigma$ is the later surface free energy (1.15 x $10^{-2}$ J/m$^2$), $\sigma_e$ is the fold surface free energy, and $k_B$ is Boltzmann's constant. The Lauritzen-Hoffmann equation can be applied to nonisothermal data to describe the crystallization kinetics.[39]

Replacing crystallization half time with peak crystallization time and isothermal crystallization temperature with peak crystallization temperature, the data in Figure 6 are plotted in Figure 7 according to eq. (2). One can see that the Lauritzen-Hoffmann equation demonstrates discontinuities for neat PP. However, no such discontinuous variation can be seen for the $TiO_2$-filled PP. The observed discontinuity may be attributed to a change in the crystallization mechanism. The Lauritzen-Hoffmann values plotted for nano-filled PP shifted to the right because of the lower supercooling degree, $\Delta T$ at which crystallization occurred.[40] To verify any possible change in the crystallization mechanism, determination of parameters at the lower cooling rates and higher cooling rates were performed (results shown in Table III). The obtained nucleation parameter ($K_g$) (from the slope of the fitting line) values can be used to calculate the fold surface free energy ($\sigma_e$) of materials from eq. (3) and the values are listed in Table III. It can be observed from Table III that the values of $K_g$ and $\sigma_e$, display a significant increase at the higher cooling range, which correspond to a lower crystallization temperature range of neat PP. In contrast, no significant change in both $K_g$ and $\sigma_e$ values for $TiO_2$-filled PP occurs. A foreign surface often reduces the nucleus size needed for crystal growth. This is because the creation of the interface between polymer crystal and substrate may be less hindered than the creation of the corresponding free polymer crystal surfaces. A heterogeneous nucleation path makes use of a foreign pre-existing surface to reduce the free energy opposing primary nucleation.[41] As a result, the value of $\sigma_e$ is reduced, thereby giving rise to an increase in crystallization rate. This indicates that $TiO_2$ can act as a very effective nucleating agent for PP, irrespective of cooling rate.

## CONCLUSIONS

This work shows the influence of $TiO_2$ nanoparticles on the crystallization process of PP using conventional DSC and flash DSC analyses in order to verify a wider range of cooling rates and crystallization temperatures. The results show that the crystallization of the α-phase and the formation of a mesophase are influenced by the presence of titania. The data obtained from both conventional DSC and flash DSC were estimated for the first time using the Lauritzen-Hoffmann theory under nonisothermal measurement. The $K_g$ and $\sigma_e$ parameters of $TiO_2$ nanoparticles-filled PP are much lower than that of neat PP, indicating that the $TiO_2$ nanoparticles serve as a very effective nucleating agent to enhance the overall crystallization rate of PP. In contrast, it retards chain mobility with higher $\Delta E$ values at cooling rates below 150 °C/s. However, it helps to make the molecular chains of PP crystallize easier during a nonisothermal crystallization process at cooling rates above 150 °C/s.

## ACKNOWLEDGMENTS

The authors thank Borealis and Huntsman for providing the materials needs for this study. We also thank Dr. L. Lin (CCe, Kaiserslautern) and V. Demchuk (PE, Hamburg-Harburg) for the compounding and injection molding of the nanocomposite samples.

## REFERENCES

1. Zhou, Z.; Wang, S.; Lu, L.; Zhang, Y.; Zhang, Y. *J. Polym. Sci. Part B: Polym. Phys.* **2007**, *45*, 1616.
2. Ruksakulpiwat, Y.; Suppakarn, N.; Sutapun, W.; Thomthong, W. *Compos. Part A* **2007**, *38*, 590.
3. Thanomchat, S.; Srikulkit, K.; Suksut, B.; Schlarb, A. K. *Int. J. Appl. Sci. Technol.* **2014**, *7*, 23.
4. Saujanya, C.; Radhakrishnan, S. *Polymer* **2001**, *42*, 4537.

5. Fu, S. Y.; Lauke, B.; Mäder, E.; Yue, C. Y.; Hu, X. *Compos. Part A* **2000**, *31*, 1117.
6. Chan, C. M.; Wu, J.; Li, J. X.; Cheung, Y. K. *Polymer* **2002**, *43*, 2981.
7. Altan, M.; Yildirim, H. *World Acad. Sci. Eng. Technol.* **2010**, *46*, 289.
8. Schlarb, A. K.; Suwitaningsih, D. N.; Kopnarski, M.; Niedner-Schatteburg, G. *J. Appl. Polym. Sci.* **2014**, *131*, DOI: 10.1002/app.39655.
9. Suksut, B.; Schlarb, A. K. *WAK* **2014**, *10*, 68.
10. Avrami, M. *J. Chem. Phys.* **1939**, *7*, 1103.
11. Avrami, M. *J. Chem. Phys.* **1940**, *8*, 212.
12. Avrami, M. *J. Chem. Phys.* **1941**, *9*, 177.
13. Lauritzen, J. I.; Hoffman, J. D. *J. Appl. Phys.* **1973**, *44*, 4340.
14. Hoffman, J. D.; Davis, G. T.; Lauritzen, Jr. J. I. In Treatise on Solid State Chemistry; Hannay, N.B., Ed.; Plenum Press: New York, **1976**; Vol. *3*, Chapter 7.
15. Huang, J. W. *Polym. Eng. Sci.* **2009**, *49*, 1855.
16. Brucato, V.; Piccarolo, S.; Carrubba, V. L. *Chem. Eng. Sci.* **2002**, *57*, 4129.
17. Minakov, A. A.; Schick, C. *Rev. Sci. Instrum.* **2007**, *78*, 073902073902.
18. Schick, C. *Anal. Bioanal. Chem.* **2009**, *395*, 1589.
19. Mathot, V.; Pyda, M.; Pijpers, T.; Poel, G. V.; van de Kerkhof, E.; van Herwaarden, S.; van Herwaarden, F.; Leenaers, A. *Thermochim. Acta* **2011**, *522*, 36.
20. Kolesov, I.; Mileva, D.; Androsch, R.; Schick, C. *Polymer* **2011**, *52*, 5156.
21. Kolesov, I.; Androsch, R.; Mileva, D.; Lebek, W.; Benhamida, A.; Kaci, M.; Focke, W. *Colloid. Polym. Sci.* **2013**, *291*, 2541.
22. Mollova, A.; Androsch, R.; Mileva, D.; Schuck, C.; Benhamida, A. *Macromolecules* **2013**, *46*, 828.
23. Schawe, J. E. K. *J. Therm. Anal. Calorim.* **2014**, *116*, 1165.
24. Wurm, A.; Herrmann, A.; Cornelius, M.; Zhuravlev, E.; Pospiech, D.; Nicula, R.; Schick, C. *Macromol. Mater. Eng.* **2015**, *300*, 637.
25. Androsch, R.; Lorenzo, M. L. D. *Polymer* **2013**, *54*, 6882.
26. Cocca, M.; Androsch, R.; Righetti, R. C.; Malinconico, M.; Lorenzo, M. L. D. *J. Mol. Struct.* **2014**, *1078*, 114.
27. Bosq, N.; Guigo, N.; Zhuravlev, E.; Sbirrazzuoli, N. *J. Phys. Chem. B* **2013**, *117*, 3407.
28. Stolte, I.; Androsch, R.; Lorenzo, M. L. D.; Schick, C. *J. Phys. Chem. B* **2013**, *117*, 15196.
29. Mollova, A.; Androsch, R.; Mileva, D.; Gahleitner, M.; Funari, S. *Eur. Polym. J.* **2013**, *49*, 1057.
30. Schawe, J. E. K. *Thermochim. Acta* **2015**, *603*, 85.
31. Schawe, J. E. K.; Vermeulen, P. A.; van Drongelen, M. *Colloid. Polym. Sci.* **2015**, *293*, 1607.
32. Luijsterburg, B. J.; de Kort, G. W.; van Drongelen, M.; Govaert, L. E.; Goossens, J. G. P. *Thermochim. Acta* **2015**, *603*, 94.
33. Androsch, R.; Lorenzo, M. L. D.; Schick, C.; Wunderlich, B. *Polymer* **2010**, *51*, 4639.
34. Kissinger, H. E. *J. Res. Nat. Bur. Stand.* **1956**, *57*, 217.
35. Spruiell, J. E.; White, J. *Polym. Eng. Sci.* **1957**, *15*, 660.
36. Hsiung, C. M.; Cakmak, M.; White, J. L. *Polym. Eng. Sci.* **1990**, *30*, 967.
37. Pérez, C. J.; Alvarez, V. A.; Stefani, P. M.; Vázquez, A. *J. Therm. Anal. Calorim.* **2007**, *88*, 825.
38. Chan, T. W.; Isayev, A. I. *Polym. Eng. Sci.* **2004**, *34*, 461.
39. Ding, Z.; Spruiell, J. E. *J. Polym. Sci. Part B: Polym. Phys.* **1997**, *35*, 1077.
40. Puente, J. A. S.; Esposito, A.; Chivrac, F.; Dargent, E. *Macromol. Symp.* **2013**, *328*, 8.
41. Mucha, M.; Królikowski, Z. *J. Therm. Anal. Calorim.* **2003**, *74*, 549.